frontiers | Frontiers in Earth Science

TYPE Original Research
PUBLISHED 20 August 2024
DOI 10.3389/feart.2024.1444690

OPEN ACCESS

EDITED BY
Jyoti Phirani,
Indian Institute of Technology Delhi, India

REVIEWED BY
Yanghui Li,
Dalian University of Technology, China
Xiangchao Shi,
Southwest Petroleum University, China

*CORRESPONDENCE
Na Wei,
weina8081@163.com
Cong Li,
202114000002@stu.swpu.edu.cn

RECEIVED 06 June 2024
ACCEPTED 06 August 2024
PUBLISHED 20 August 2024

CITATION
Wei N, Li C, Zhao X, Li H, Zhang L, Zhao J, Kvamme B and Coffin RB (2024) Numerical simulation of depressurization exploitation in class 1 hydrate reservoirs under different development factors in Shenhu area, South China sea.
Front. Earth Sci. 12:1444690.
doi: 10.3389/feart.2024.1444690

Numerical simulation of depressurization exploitation in class 1 hydrate reservoirs under different development factors in Shenhu area, South China sea

Na Wei[1,2]*, Cong Li[1,2]*, Xingxin Zhao[1,2], Haitao Li[1,2], Liehui Zhang[1,2], Jinzhou Zhao[1,2], Bjørn Kvamme[1,2] and Richard B. Coffin[1,2]

[1]State Key Laboratory of Oil and Gas Reservoir Geology and Exploitation, Southwest Petroleum University, Chengdu, China, [2]State Key Laboratory of Natural Gas Hydrate, Beijing, China

Most of the implemented marine gas hydrate test exploitation in the world adopt the depressurization method to break down the hydrate in the reservoir into natural gas and then extract it, but because the gas production results are still a certain distance away from the commercial exploitation, and it mainly stays in the stage of theoretical research and trial exploitation. Based on two trial productions in the Shenhu area of the South China Sea, this study established a model for hydrate exploitation and investigated the impact of different well types on the recovery rates of hydrates and free gas in different development layers during depressurization. For the Class 1 hydrate reservoirs, horizontal wells are the optimal solution to extract hydrate and free gas simultaneously when exploiting the hydrate three-phase layer. Meanwhile, the effect of different well spacing in vertical wells on the recovery rate of hydrate and free gas was studied. It is found that the best recovery efficiency is achieved when the spacing between two wells is 80 m. The lower the bottom flow pressure of the well, the higher the production capacity, but its influence is limited.

KEYWORDS

class 1 hydrate reservoirs, depressurization exploitation, numerical simulation, recovery rate, horizontal well

1 Introduction

Natural gas hydrate (NGH), commonly known as combustible ice, is a clathrate crystalline compound formed by hydrocarbon gases such as methane and water under high pressure and low temperature (McMullan and Jeffrey, 1965; Sloan and Koh, 2007). NGH has the characteristics of high energy density, wide distribution, large scale, high combustion value, clean and no pollution, etc. It is an energy source that has not yet been effectively developed on a large scale on earth and is also known as the new alternative energy source with the most development potential in the 21st century (Xu and Li, 2015; Chibura et al., 2022; Wei et al., 2022). The efficient development of hydrate resources from marine sediments is crucial in addressing the world's energy shortage (Zhao et al., 2017; Xu et al., 2019; Wei et al., 2021).

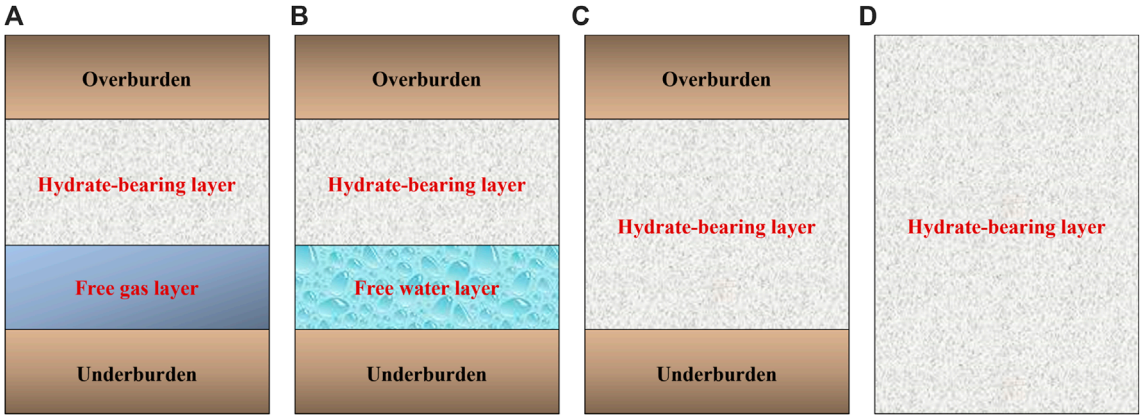

FIGURE 1
Classification of natural gas hydrate reservoirs. **(A)** Class 1, **(B)** Class 2 **(C)** Class 3 **(D)** Class 4.

Moridis et al. divided the natural hydrate accumulations into four main classes that are defined by their geologic features and their initial conditions (Moridis and Collett, 2003; Moridis and Reagan, 2007a; Moridis and Reagan, 2007b; Moridis et al., 2007; Moridis and Sloan, 2007), and most of the current studies have been conducted based on this classification. As shown in Figure 1, the Class 1 accumulations are composed of two layers: the Hydrate-Bearing Layer (hereafter referred to as HBL) and an underlying two-phase fluid layer containing gas and liquid water. In Class 1 deposits, the bottom of the HBL occurs under equilibrium conditions and defines the bottom of the stability zone. In addition, depending on the composition of the HBL, it is divided into two types: water-saturated (Class 1W) and gas-saturated (Class 1G) (Moridis and Reagan, 2011a). In Class 2 deposits, an HBL overlies a layer of mobile water. Class 3 accumulations are composed of a single zone, the hydrate interval (HBL), and are characterized by the absence of an underlying zone of mobile fluids. A fourth class (Class 4) involves exclusively oceanic systems, and involves dispersed, low-saturation hydrate deposits that lack confining geologic strata. Among them, the Class 1 accumulations are currently the preferred target for hydrate exploitation because the temperature and pressure conditions in this class of hydrate reservoir are close to the phase equilibrium line, meaning that only a small amount of decomposition driving force is required for hydrate decomposition. Additionally, the Class 1 hydrate reservoirs have the advantage that even if the hydrate decomposition is minimal, a certain amount of gas can still be recovered during exploitation due to the underlying free gas.

Natural gas hydrates are extracted by decomposing solid hydrates into water and methane gas in the reservoir environment, and then collecting the methane gas through extraction wells. Currently, the exploitation methods of natural gas hydrate mainly include depressurization (Wang et al., 2013; Zhao et al., 2015), thermal stimulation (Cranganu, 2009; Nair et al., 2016), inhibitor injection (Li et al., 2007; Villano et al., 2009), N_2/CO_2 replacement (Ohgaki et al., 1996; Goel, 2006), and solid fluidization exploitation methods proposed for the development of marine non-diagenetic natural gas hydrate (Zhou et al., 2014; Zhou et al., 2017; Wei et al., 2018; Zhou et al., 2018). Of these methods, depressurization and heating methods are relatively simple to implement. However, compared to the heating method, depressurization is more cost-effective and has higher gas production efficiency. It is the main method used in recent test exploitation and will be the primary method for gas hydrate exploitation in the future. During production in the Messoyakha hydrate reservoirs, depressurization was the dominant mechanism (Makogon and Omelchenko, 2013). The first oceanic hydrate production trial in the Eastern Nankai Trough achieved a gas production rate of 20,000 m^3/d via depressurization (Yamamoto, 2015). China conducted two trial productions in the Shenhu Area of the South China Sea in 2017 and 2020, respectively. The first trial production used straight wells for depressurization development, and the average daily gas production was only 5,151 m^3/d (Li et al., 2018), while the second trial production used horizontal wells for depressurization development, and the average daily gas production increased significantly to 2.87×10^4 m^3/d (Ye et al., 2020).

Due to the complexity, high investment, and unpredictability of hydrate test exploitation projects, it is beneficial to use powerful, flexible, and cost-effective numerical simulation research methods to pre-evaluate hydrate reservoirs before their extraction (Moridis, 2003; Konno et al., 2017). Various widely used hydrate simulators, including TOUGH + HYDRATE (T + H) (Moridis et al., 2011; Sun et al., 2019), HydrateResSim (Gamwo and Liu, 2010), MH21-HYDRES (Masuda et al., 2008; Kurihara et al., 2009), STOMP-HYD (Anderson et al., 2011), and CMG-STARS (Myshakin et al., 2012; Lin et al., 2020), can be utilized to analyze the hydrate production performance and determine exploitation strategy preferences. At present, many numerical simulation studies have been carried out on the depressurization production of natural gas hydrate reservoirs.

Hong and Pooladi-Darvish (2003) simulated the depressurization u7production of a two-dimensional cylindrical natural gas hydrate reservoir, studied the influence of various parameters on gas production behavior, and analyzed the natural gas production potential of gas hydrate bearing formation. Moridis and Reagan analyzed the production performance of hydrate reservoir under different heat injection and depressurization conditions. Li et al. (2011) established a single hydrate reservoir production model and discussed the gas production efficiency of

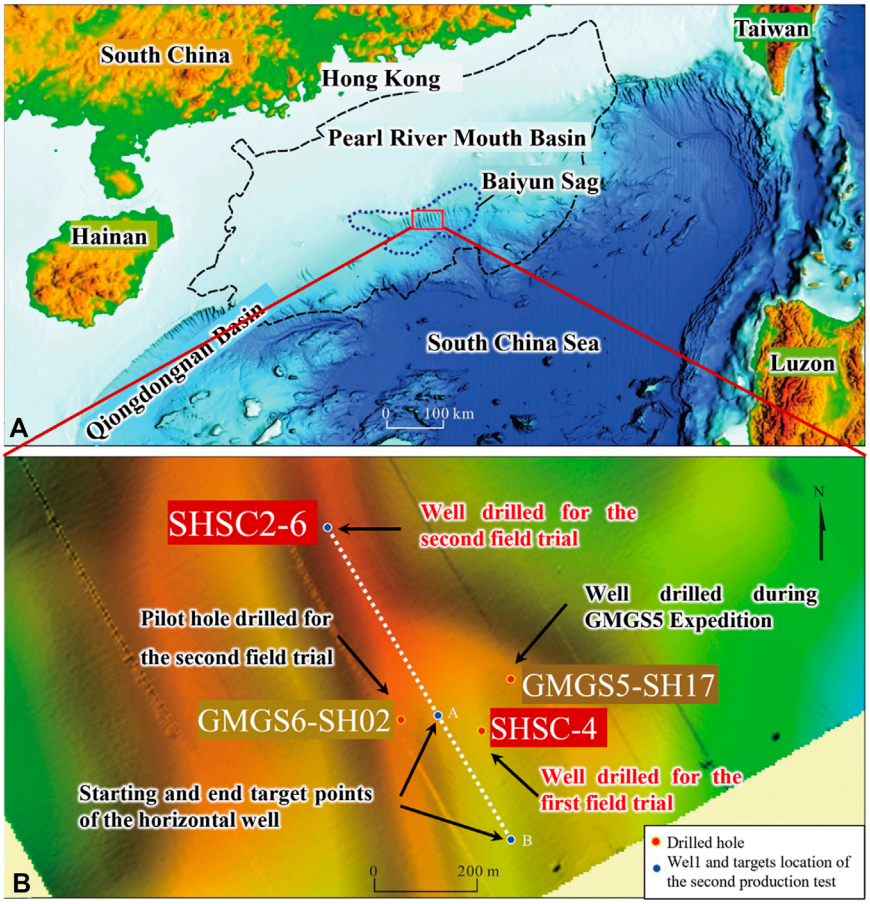

FIGURE 2
The regional geological setting and location of the two offshore NGH production test sites. The red rectangle in **(A)** indicates the production test area. **(B)** illustrates the topography surrounding the production well and the trajectory of the well (Yu et al., 2021).

depressurization production in horizontal wells. In 2011, Moridis and Reagan et al. (2011b) used the T + H to perform depressurizing dissociation simulations of actual geological gas hydrate reservoirs. The calculation results show that the gas production phase can be divided into two phases. The first is the phase where the gas production gradually increases, and the water production gradually decreases, and the second is the phase where the fluid production rate is very low. Moridis also compared the performance of a vertical well and a horizontal well and found that production using horizontal wells is approximately two orders of magnitude larger than that from vertical wells accessing the same section of the HBL. In 2012, Su et al. (2012) established a vertical shaft depressurization mining model using T+H study based on the real geological parameters in the Shenhu Sea, South China Sea. The simulation results showed that the proportion of hydrate decomposition produced water was too large when the vertical wells were mined by depressurization, and the area could not be mined economically and efficiently by using the depressurization method alone. In 2015, Feng et al. (2015) compared the hydrate production efficiency of single horizontal and double horizontal wells. In 2018, Chen et al. (2018) tablished a geological model for the hydrate trial production area in the Shenhu Sea area of the South China Sea and predicted the potential production behavior of the area. In 2022, Guo et al. (2022) demonstrated that the recovery rates of hydrate and free gas are significantly influenced by well placement and stimulation in different development configurations.

In 2021, Yu et al. (2019) further investigated the free gas accumulation behavior in a methane hydrate reservoir by using a multiple-well system with an assumed WS. They found that the free gas accumulation zone was dramatically enlarged with the increase in well spacing, which means a proper WS should be carefully determined. Similarly, Terzariol and Santamarina. (2021) also studied reasonable well spacing under the condition of multi-well depressurization production of hydrate to explore the synergistic interactions among wells. Their investigation also indicated the optimal WS is mainly dependent on the characteristic lengths, burdens permeability, well pressure, and formation thickness. In 2023, Sun et al. (2023) compared the production performance of vertical and horizontal wells with different well spacing. The results show that the relatively longer WS in homogeneous sediments with the same ultra-low permeability means lower cumulative gas recovery, but the full opposite phenomenon will be observed after increasing the formation permeability, and subsequently, a method to determine the

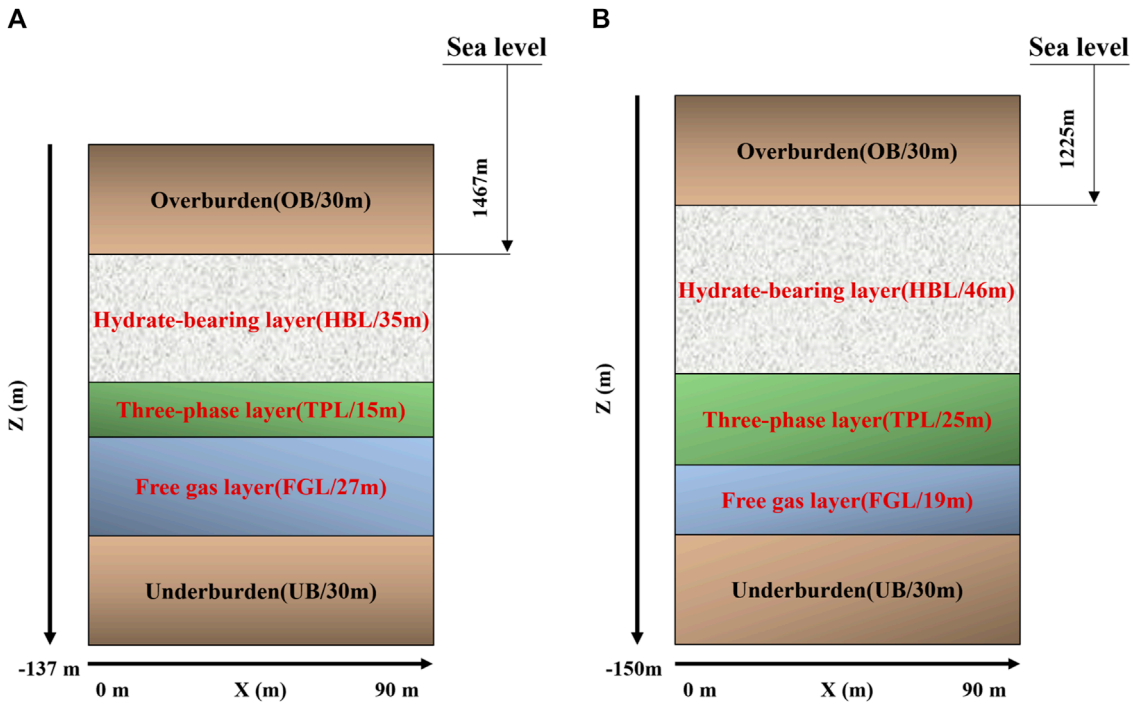

FIGURE 3
Construction of the class 1 hydrate reservoirs model for depressurization exploitation in the Shenhu Sea, South China Sea. **(A)** Hydrate reservoir model, 2017. **(B)** Hydrate reservoir model, 2020.

optimal well spacing by the minimum radius of curvature method was proposed.

In 2013, Zhao et al. (2013) used T + H to numerically simulate the gas production potential of a single vertical well gas hydrate reservoir in the Qilian Mountain permafrost zone of the Qinghai-Tibet Plateau with bottomhole pressures of 1, 1.5, and 2.5 MPa, respectively. The results suggest that lower production pressures may not be conducive to exploiting the gas production potential of hydrate reservoirs. Fan et al. (2013) utilized the HydrateResSim simulator to model a horizontal well for hydrate extraction under constant temperature and pressure reduction, defining three pressure scenarios to analyze heat injection efficiency and gas production rates. Results indicated that the hydrate gas production rate increased over time before stabilizing, with higher pressure reductions leading to increased production capacity. In 2017, Merey and Sinayuc et al. (2017) performed pressure reduction mining analyses on hydrate reservoirs of varying thicknesses using the HydrateResSim simulator for pressure reductions ranging from 2.0 to 6.0 MPa. Xia et al. (2019) introduced a novel depressurization mode with decreasing bottom-hole pressure in 2020, investigating its production characteristics numerically. They discovered that as the depressurization exponent decreased, gas production, dissociation, and the gas-to-water ratio all increased. Compared to the proposed depressurization model, the index for hydrate production at constant bottom-hole pressure was better; however, it resulted in higher energy consumption within the hydrate reservoir and more severe hydrate alteration. Therefore, a suitable depressurization exponent should be selected to achieve a balance between production and reservoir energy consumption during depressurization production.

In summary, despite numerous preliminary evaluations conducted on various well types, well spacings, and bottomhole pressures, systematic discussions on the impact of different production intervals on hydrate recovery rates, particularly for Type 1 hydrate reservoirs, remain scarce. This study not only updates the simulation benchmarks based on the latest trial production data but also systematically investigates the effects of distinct development intervals on the recovery rates of Type 1 hydrate reservoirs. Through a comparative analysis of two hydrate trial production campaigns conducted in the Shenhu area of the South China Sea in 2017 and 2020, this research, for the first time, elaborates on the specific impacts of well types and development intervals on the recovery rates of hydrates and free gas, which have often been overlooked in previous studies. Furthermore, we assess the influence of varying well spacings for vertical wells on production performance, offering fresh insights into optimizing well spacing designs. Unlike previous studies that primarily focused on geological factors, our research underscores the significance of development factors, such as well type selection and production strategies, in enhancing recovery rates, and it presents, for the first time, an Inflow Performance Relationship (IPR) curve for hydrate production. These novel findings provide vital engineering references for the development of hydrate reservoirs in the South China Sea and other maritime regions worldwide, particularly in implementing depressurization-based extraction projects.

TABLE 1 Parameters and models used in the simulations (Li et al., 2018; Ye et al., 2020).

Parameter	Value and model	
Year	1st test (2017)	2nd test (2020)
Water depth (m)	1,266	1,225
Reservoir depth (mbsf)	200–278	207–297
Reservoir thickness (m)	78	90
The hydrate-bearing layer thickness (m)	35	46
The hydrate three-phase layer thickness (m)	15	25
The free gas layer thickness (m)	27	19
Initial temperature at the bottom of the three-phase layer (°C)	15.12	16.15
Initial pressure at the bottom of the three-phase layer (MPa)	15.05	15.95
Geothermal gradient (°C/100 m)	5.4	5.4
Average hydrate saturation in hydrate-bearing layer (%)	34	31
Average hydrate saturation in hydrate three-phase layer (%)	31	11.7
Average gas saturation in hydrate three-phase layer (%)	16.4	13.2
Average gas saturation in free gas layer (%)	7.8	7.3
Average permeability of hydrate-bearing layer (mD)	2.9	2.38
Average permeability of hydrate three-phase layer (mD)	1.5	6.63
Average permeability of free gas layer (mD)	7.4	6.8
Average porosity of hydrate-bearing layer (%)	35	37.3
Average porosity of hydrate three-phase layer (%)	33	34.6
Average porosity of free gas layer (%)	32	34.7
Relative permeability model	$K_{rA} = (S_A\text{-}S_{irA})/(1\text{-}S_{irA})^n$	
	$K_{rG} = (S_G\text{-}S_{irG})/(1\text{-}S_{irA})^{nG}$	
Composite thermal conductivity model	$K_\theta = K_{\theta RD} + \left(S_A^{1/2} + S_H^{1/2}\right) \times (K_{\theta RW}\text{-}K_{\theta RD}) + \varphi S_I K_{\theta I}$	
λ, P_0, n, n_G, S_{irA}, S_{irG}	0.30, 10^5 Pa, 3.5, 2.5, 0.3, 0.05	

2 Mathematical model

2.1 T + H code introduction

The TOUGH+HYDRATE code (T+H) was developed by the Lawrence Berkeley National Laboratory (LBNL) in the United States and has been extensively used internationally in the field of hydrates. T + H is a fully implicit compositional simulator that accounts for four phases (gas, water, ice, hydrate) as well as three components (CH_4, H_2O, NaCl), to simulate the decomposition and formation processes of hydrates under different exploitation modes, equilibrium conditions, and kinetic conditions. By solving the coupled mass-energy balance equations and satisfying Darcy's law, T+H can simulate the coupled processes of phase transition, heat transfer, and multiphase flow during hydrate extraction in natural gas hydrate deposits (Moridis and Reagan, 2007b).

2.2 Model assumptions

The assumptions in this model are listed as follows (Moridis and Reagan, 2007b). 1) Hydrate is a single methane hydrate with a methane content of 100%. 2) Darcy's law is valid in the simulated domain under the conditions of the study. 3) Neglecting the mechanical dispersion of dissolved gases and inhibitors in the aqueous phase during transport, disregarding molecular diffusion and hydrodynamic diffusion. 4) Dissolved salts do not precipitate as their concentration increases during water freezing. 5) The concentration of the dissolved inhibitors is such that it does not affect the thermophysical properties of the aqueous phase. 6) Inhibitors do not react with reservoir minerals. 7) The pressure $P < 100$ MPa (14,504 psi).

2.3 Mathematical model in T+H code

In the T + H code, mass and heat balance considerations in every subdomain (gridblock) into which the simulation domain is been subdivided by the integral finite difference method dictate that:

$$\frac{d}{dt}\int_{V_n} M^k dV = \int_{\Gamma_n} \mathbf{F}^k \cdot \mathbf{n} d\Gamma + \int_{V_n} q^\kappa dV \tag{1}$$

where V_n is volume of subdomain n, m^3; M^k is mass accumulation term of component κ, $kg{\cdot}m^{-3}$; κ is hydrate(h) or methane (m) or water (w) or water-soluble inhibitor (i) or heat (θ); $\mathbf{F}^k$ is Darcy flux vector of component κ, $kg{\cdot}m^{-2}{\cdot}s^{-1}$; Γ_n is surface area of subdomain n, m^2; $\mathbf{n}$ is inward unit normal vector; q^κ is source/sink term of component κ, $kg{\cdot}m^{-3}{\cdot}s^{-1}$; t is time, s.

Under equilibrium conditions, the mass accumulation terms M^k in Equation 1 is given by Equation 2 below.

$$M^\kappa = \sum_{\beta \equiv A,G,I,H} \phi S_\beta \rho_\beta X_\beta^\kappa, \kappa \equiv w, m, i \tag{2}$$

where ϕ is porosity, dimensionless; β is solid-hydrate (H) or aqueous (A) or gaseous (G) or solid-ice (I); S_β is saturation of phase β, dimensionless; ρ_β is density of phase β, $kg{\cdot}m^{-3}$; X_β^κ is mass fraction of component $\kappa \equiv w, m, i$ in phase β, kg/kg.

The mass fluxes of water, CH_4, and inhibitor include contributions from the aqueous and gaseous phases, are shown in Equation 3.

$$\mathbf{F}^\kappa = \sum_{\beta \equiv A,G} \mathbf{F}_\beta^\kappa, \kappa \equiv w, m, i \tag{3}$$

because they are immobile, the contributions of the two solid phases ($\beta \equiv I, H$) to the fluid fluxes are zero. The heat flux accounts for conduction, advection, and radiative heat transfer, and is given by Equation 4.

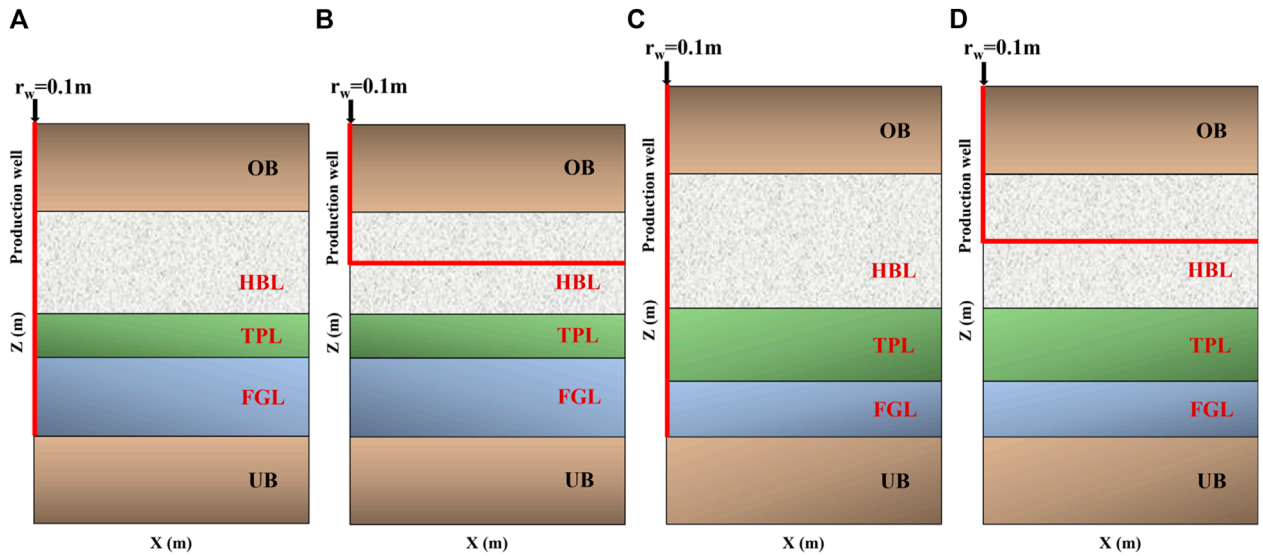

FIGURE 4
Schematic diagram of production well design for two offshore NGH production test in the Shenhu Sea, South China Sea. **(A)** Vertical well model 2017. **(B)** Horizontal well model 2017. **(C)** Vertical well model 2020. **(D)** Horizontal well model 2020.

$$\mathbf{F}^{\theta} = -\overline{k_{\theta}}\nabla T + f_{\sigma}\sigma_0\nabla T^4 + \sum_{\beta\equiv A,G} h_{\beta}\mathbf{F}_{\beta} \tag{4}$$

where $\overline{k_{\theta}}$ is composite thermal conductivity of the medium/fluid ensemble, $W\cdot m^{-1}\cdot K^{-1}$; h_{β} is specific enthalpy of phase $\beta \equiv A, G$, $J\cdot kg^{-1}$; f_{σ} is radiance emittance factor, dimensionless; σ_0 is Stefan-Boltzmann constant, Stefan-Boltzmann constant, 5.6687×10^{-8} $J\cdot m^{-2}\cdot K^{-4}$.

Under equilibrium conditions, the rate of heat removal or addition includes contributions of the heat associated with fluid removal or addition, as well as direct heat inputs or withdrawals, and is described by Equation 5.

$$q^{\theta} = q_d + \sum_{\kappa\equiv A,G} h_{\beta}q_{\beta} \tag{5}$$

where q_{β} is the production rate of the phase β, $kg\cdot m^{-3}$. For a prescribed production rate, the phase flow rates q_{β} are determined internally according to the general different options available in the TOUGH+ code.

Under different temperature and pressure conditions, hydrate systems are in different phase states. When the equilibrium state is broken, the state of the system will change. For the phase equilibrium relationship between hydrate decomposition and formation, Moridis (2023) has established a regression equation based on data from several researchers reported by Sloan:

$$\ln(p_e) = \begin{cases} -1.941\times10^5 + 3.310\times10^3 T - 2.255\times10^1 T^2 \\ +7.675\times10^{-2}T^3 - 1.304\times10^{-4}T^4 + 8.861\times10^{-8}T^5 \\ (T \geq 273,2K) \\ -4.389\times10^1 + 7.763\times10^{-1}T - 7.273\times10^{-3}T^2 \\ +3.854\times10^{-5}T^3 - 1.037\times10^{-7}T^4 + 1.099\times10^{-10}T^5 \\ (T < 273.2K) \end{cases} \tag{6}$$

The effect of salinity on the dissociation equilibrium pressure-temperature relationship is described by

$$T_e = T + \Delta T_D \tag{7}$$

where:

$$\Delta T_D = \Delta T_{D,r}\frac{\ln\left(1 - X^c_{mol,A}\right)}{\ln\left(1 - X^c_{mol,A,r}\right)} \tag{8}$$

In Equations 6–8, T is temperature, K; p_e is equilibrium pressure at temperature T, Pa; T_e is equivalent equilibrium temperature in the presence of inhibitor, K; ΔT_D is inhibitor-induced temperature depression, K; $\Delta T_{D,r}$ is temperature depression at the reference mole fraction $X^c_{mol,A}$, K; $X^c_{mol,A}$ is mole fraction of the inhibitor in the aqueous phase; $X^c_{mol,A,r}$ is reference mole fraction of the inhibitor in the aqueous phase; The inhibitor studied in this article is NaCl.

3 Geological setting and model construction

3.1 Geological setting

In 2015 and 2016, the China Geological Survey identified eight hydrate deposits containing underlying free gas in the Shenhu area, located on the northern slope of the Baiyun Sag within the Pearl River Mouth Basin in the northern South China Sea, as depicted in Figure 2A. Among these, the W11 and W17 deposits were selected as the optimal targets for production testing. The W17 site, situated in the Baiyun Sag of the Pearl River Mouth Basin, features a complex seabed terrain characterized by a higher north and lower south elevation, along with typical geological features such as seamounts, erosional channels, steep slopes, and reverse slopes.

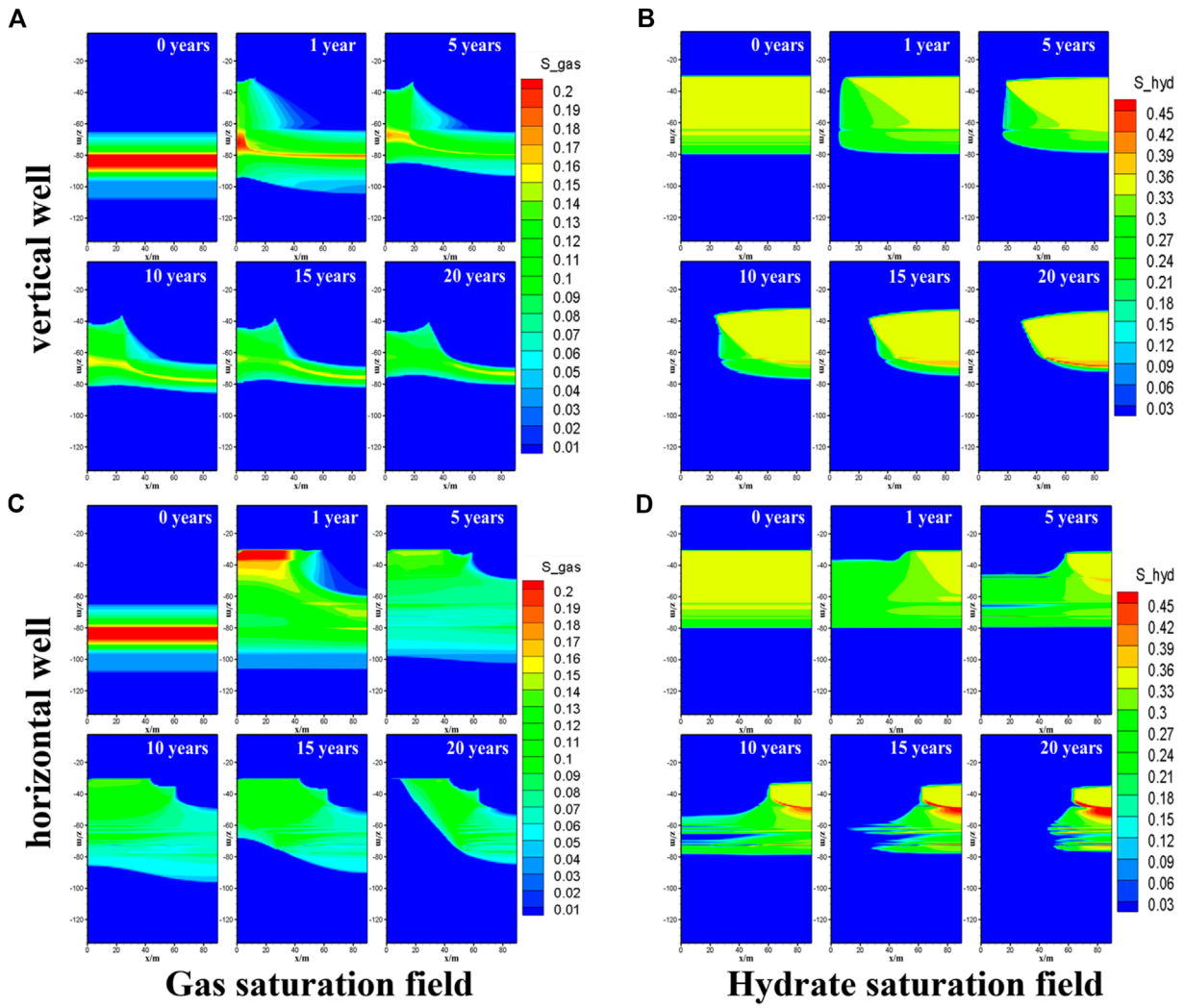

FIGURE 5
Temporal and spatial evolution of exploitation in different well types, 2017. **(A, C)** Gas saturation Field. **(B, D)** Hydrate Saturation field.

Geological and tectonic activities have resulted in the formation of a system of steeply inclined fractures and fault zones, providing favorable conditions for the formation and accumulation of natural gas hydrates. The first hydrate production test was conducted at Well SHSC-4 in the W17 site in 2017, followed by a second test at Well SHSC2-6, located approximately 500 m northwest of the first well, in 2020. The locations of the test wells are illustrated in Figure 2B. The simulated target reservoir is composed primarily of muddy silt with mineral composition mainly consisting of quartz feldspar, carbonate, and clay minerals, and its bound water saturation of the reservoir is 65% or higher. The hydrate reservoir at this station contains upper and lower capping layers, hydrate two-phase layer (water + hydrate), hydrate three-phase layer (water + hydrate + free gas), and underlying free gas layer (water + free gas), belonging to the Class1 hydrate reservoir (Li et al., 2018). It has been reported that the natural gas hydrates in the Shenhu Area of the South China Sea originate from thermogenic gas sources and occur in the form of structure I and structure II pore-filling types with methane content of over 99% (Qin et al., 2020; Ye et al., 2020; Yu et al., 2021).

3.2 Model construction

This study constructed a rectangular hydrate reservoir model (i.e., x-y-z coordinate system) for the first and second tests in the Shenhu Sea based on the field data obtained from the tests site, as illustrated in Figure 3. Figure 3A presents the geological model of the first test exploitation. From the reservoir characteristics shown in Table 1, it can be known that the marine hydrate reservoir at this site is located 200–278 m beneath the seafloor (mbsf) where the water depth is 1,266 m and the reservoir thickness is 78 m. Considering the symmetrical characteristic, only half of the reservoir model was taken into account. Furthermore, it was assumed that the reservoir properties were uniform along the y-coordinate, so only a planar reservoir model (i.e., xz coordinate system) was used as the simulation domain. This reservoir model had a length of 90 m and a height of 137 m. Along the z-coordinate, it was split into five layers from top to bottom: i) overburden (OB, 30 m); ii) hydrate-bearing layer (HBL, 35 m); iii) three-phase layer (TPL, 15 m); (iv) free gas layer (FGL, 27 m); and v) underburden (UB, 30 m). Figure 3B

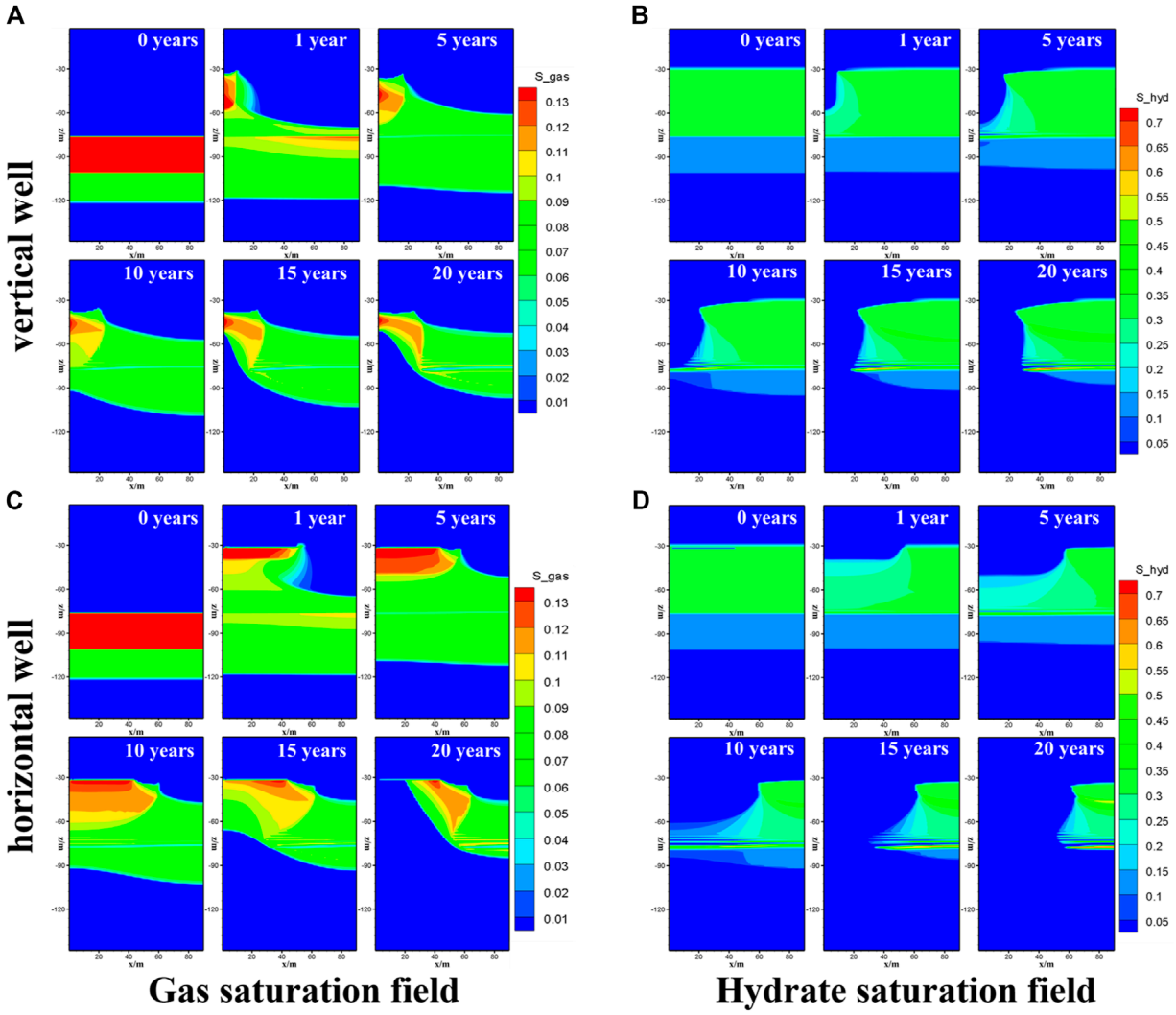

FIGURE 6
Temporal and spatial evolution of exploitation in different well types, 2020. **(A, C)** Gas saturation Field. **(B, D)** Hydrate Saturation field.

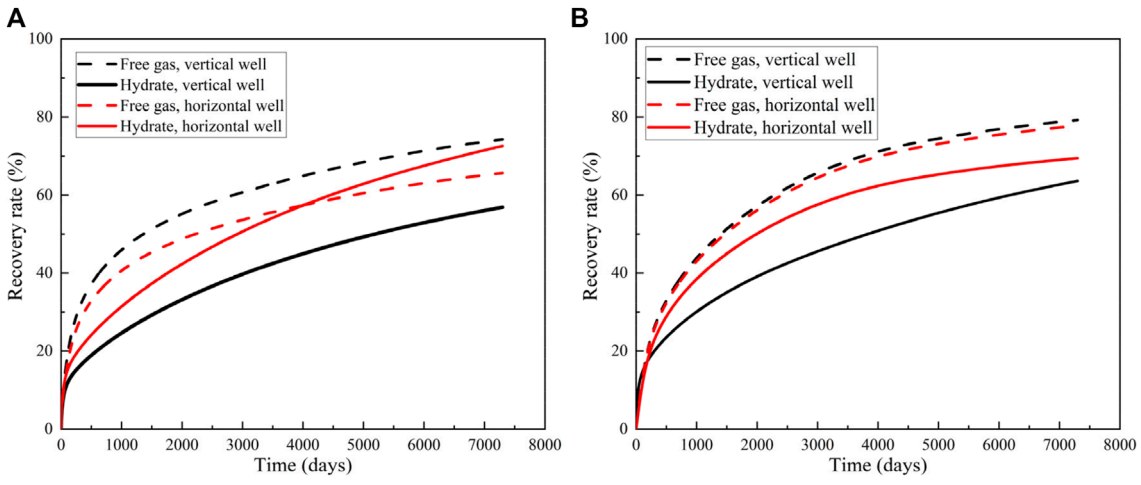

FIGURE 7
Recovery curves of free gas and hydrate from different well types in 2017 and 2020. **(A)** 2017 **(B)** 2020.

TABLE 2 Production well design of different well types and exploitation layers.

Cases	Design	Remarks
Case 1	Vertical well, HBL	Figure 8A
Case 2	Vertical well, HBL + TPL	Figure 8B
Case 3	Vertical well, HBL + TPL + FGL	Figure 8C
Case 4	Horizontal well, HBL	Figure 8D
Case 5	Horizontal well TPL	Figure 8E
Case 6	Horizontal well, FGL	Figure 8F

depicts the geological model of the second test exploitation. From the reservoir characteristics shown in Table 1, it can be known that the marine hydrate reservoir at this site is located 207–297 m beneath the seafloor (mbsf) where the water depth is 1,225 m and the reservoir thickness is 90 m. This reservoir model had a length of 90 m and a height of 150 m. Along the z-coordinate, it was split into five layers from top to bottom: i) overburden (OB, 30 m); ii) hydrate-bearing layer (HBL, 46 m); iii) three-phase layer (TPL, 25 m); iv) free gas layer (FGL, 19 m); and v) underburden (UB, 30 m).

The initial conditions and boundary conditions of the reservoir for this numerical simulation are from the public data of two tests in the Shenhu Sea, South China Sea, and the specific data are shown in Table 1. The survey shows that the seafloor temperature in the Shenhu sea area is 3.3–3.7°C, the heat flux is 74–78 mW/m^2, and the geothermal gradient is 4.3–6.77°C/100 m.30,31 Therefore, we set the initial temperature at the bottom of TPL for the first and second tests models to 15.12°C and 16.15°C the initial pressure at the bottom of TPL to 15.05 MPa and 15.95 MPa, and the geothermal gradient was set to 5.4°C/100 m. The OB and UB only contained liquid water without any free gas or hydrates, and since the corresponding reservoir conditions (i.e., average porosity and permeability) have not been reported in the literature, they were assumed to be identical with those of the HBL and FGL. In addition, the gas that formed the natural gas hydrates in the reservoir model was assumed to be 100% methane.

4 Results and discussion

4.1 Effect of well type

According to publicly available information, the second test recovery yielded 5.57 times the daily gas production of the first test recovery. To investigate whether the significant increase in gas production was due to the well type factor, numerical simulations of vertical and horizontal well extraction were carried out using the geological parameters of the first and second test production, respectively. The physical models established are illustrated in Figure 4.

Figure 5 display the spatial and temporal evolution of the gas phase saturation field and hydrate saturation field during the first test exploitation, while Figure 6 illustrate the spatial and temporal evolution of the second test exploitation. The left two panels of the figure depict the changes in gas saturation during the production process, while the right two panels show the corresponding changes in hydrate saturation. As seen in Figure 5A, initially, there are significant differences in gas saturation and pressure gradients between layers, allowing free gas to rapidly disperse near the well. However, after 20 years, the dispersion becomes limited to the immediate vicinity of the well. Figure 5C reveals that during the early stages of gas production, the exploitation of the two-phase hydrate layer using a horizontal well results in significant migration of free gas into this layer. After 20 years of gas production, all free gas in the free gas layer near the well is recovered, yet a considerable amount of free gas remains in the two-phase hydrate layer. Figures 5B–D indicate that hydrate decomposition initiates near the wellbore during the initial stages of production using both vertical and horizontal wells. In the case of vertical well production, hydrates surrounding the well are initially extracted by disrupting their equilibrium state, leading to a significantly larger area of undecomposed hydrates remaining after 20 years of gas production compared to that observed in horizontal well production.

Figure 6 show that the spatial and temporal evolution patterns of the gas phase saturation field and hydrate saturation field during both vertical and horizontal well exploitation observed in 2020 are comparable to those in 2017. Thus, we will not discuss them further here. Nonetheless, it is worth noting that the final remaining areas of free gas and undecomposed hydrate zone differ significantly due to the distinct geological conditions.

In addition, Figure 7 shows the variation of the recovery rate over a 20-year mining period for both tests. Figure 7A illustrates the recovery rates of hydrate and free gas from vertical and horizontal wells during the first test in 2017. The recovery rate initially increases rapidly during the early stage of depressurized extraction, followed by a slower growth rate. After 20 years of depressurized extraction, the free gas recovery rate and hydrate recovery rate are 74.52% and 56.88%, respectively, for vertical wells, and 65.65% and 72.57%, respectively, for horizontal wells. The recovery rate of free gas from vertical wells is 8.87% higher than that from horizontal wells, while the recovery rate of hydrate from vertical wells is 15.69% lower than that from horizontal wells. In Figure 7B, the recovery rates of hydrate and free gas from vertical and horizontal wells during the second test in 2020 are presented. After 20 years of reduced pressure extraction, the free gas recovery rate is 79.22% and the hydrate recovery rate is 63.62% for vertical wells, while the free gas recovery rate is 77.77% and the hydrate recovery rate is 69.44% for horizontal wells. The recovery rate of free gas from vertical wells is 1.45% higher than that from horizontal wells, and the recovery rate of hydrate from vertical wells is 5.82% lower than that from horizontal wells. Based on these results, we can conclude that extracting the hydrate layer is more economically efficient as the hydrate saturation is much higher than the free gas saturation. Therefore, we recommend using horizontal wells for the exploitation of the Class 1 hydrate reservoir under depressurization.

4.2 Effect of exploitation layer

Due to the abundance of numerical simulations on the first trial production in 2017, there are relatively fewer numerical simulations for the second trial production in 2020. Starting from this section, numerical simulations will be conducted for the second

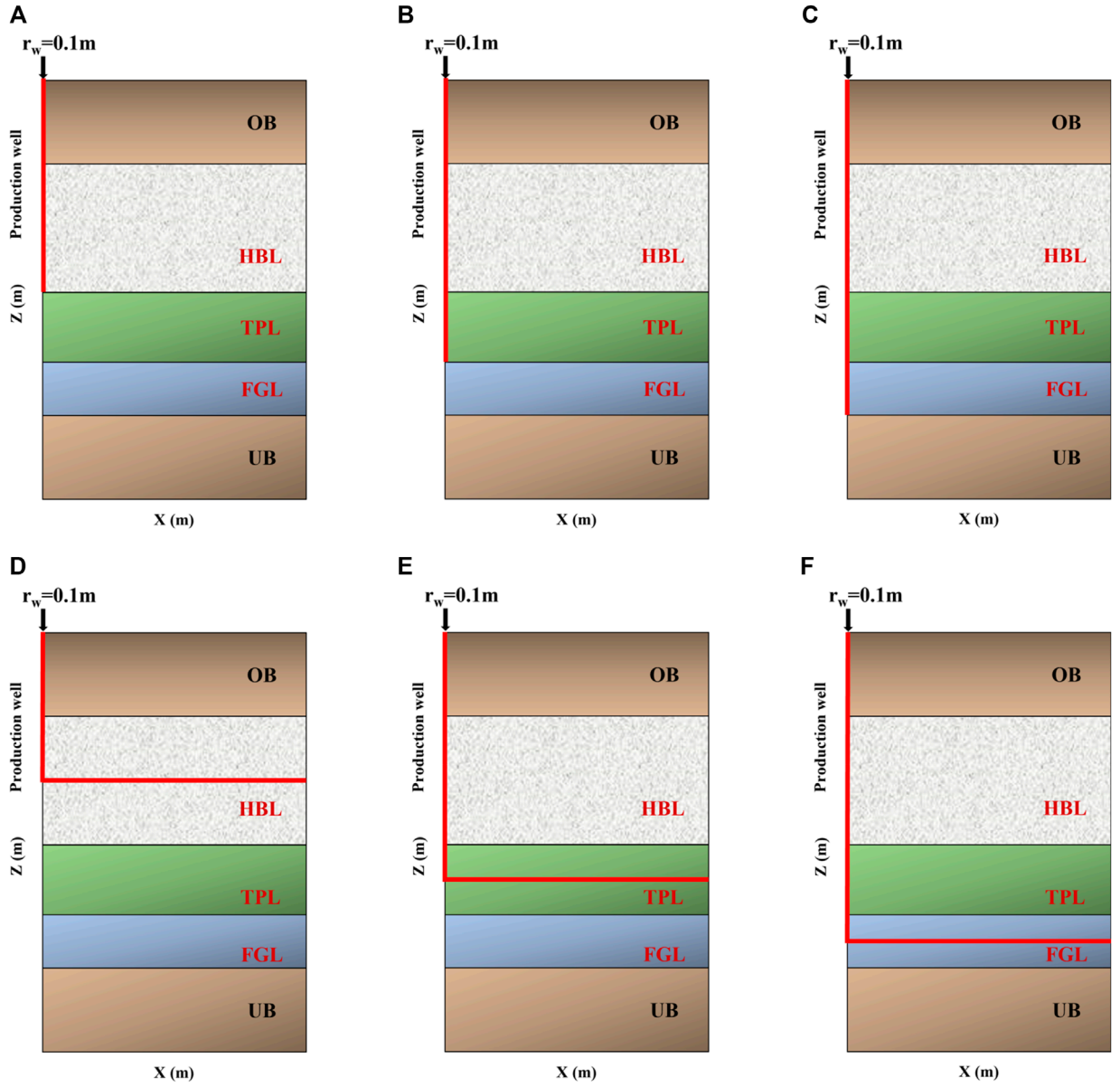

FIGURE 8
Schematic diagram of production well design of different well types and exploitation horizon. **(A)** Class 1, **(B)** Class 2 **(C)** Class 3 **(D)** Class 4. **(E)** Class 5. **(F)** Class 6.

trial production in 2020. In order to investigate the effects of different well types and different production layers on the recovery rate of hydrate and free gas, this section establishes a depressurization production model with different well types and different production layers and analyzes the changes in the recovery rate of hydrate and free gas. The design of the scheme is shown in Table 2, and the model is shown in Figure 8.

The recovery rates of different scenarios over a 20-year period of exploitation are presented in Figure 9. As can be seen from Figure 9A, Case 1 results in a recovery rate of 48.35% for free gas and 38.96% for hydrate. In Case 2, the recovery rates increase to 76.55% and 58.40% for free gas and hydrate, respectively. Case 3 yields even higher recovery rates of 79.22% and 63.62% for free gas and hydrate, respectively. The recovery rates of free gas and hydrate are the highest when the straight wells are exploited to the free gas layer, while the recovery rates of free gas and hydrate are the lowest when the hydrate two-phase layer is exploited. Therefore, direct wells are recommended to reach the free gas layer. From Figure 9B, it is evident that after 20 years of exploiting horizontal wells, Case 4, which exploits the hydrate two-phase layer, results in the highest hydrate recovery rate of 74.55%, but the lowest free gas recovery rate of 57.63%. This is because the reservoir permeability is low, and the horizontal wells are not directly in contact with the free gas layer, making it difficult for the free gas to flow upward. Therefore, the gas produced by exploiting the hydrate two-phase layer is mainly hydrate decomposed gas. Case 5, on the other hand, exploits the free gas layer, resulting in the highest free gas recovery rate of 84.61%, but the lowest hydrate recovery rate of 42.26%. This

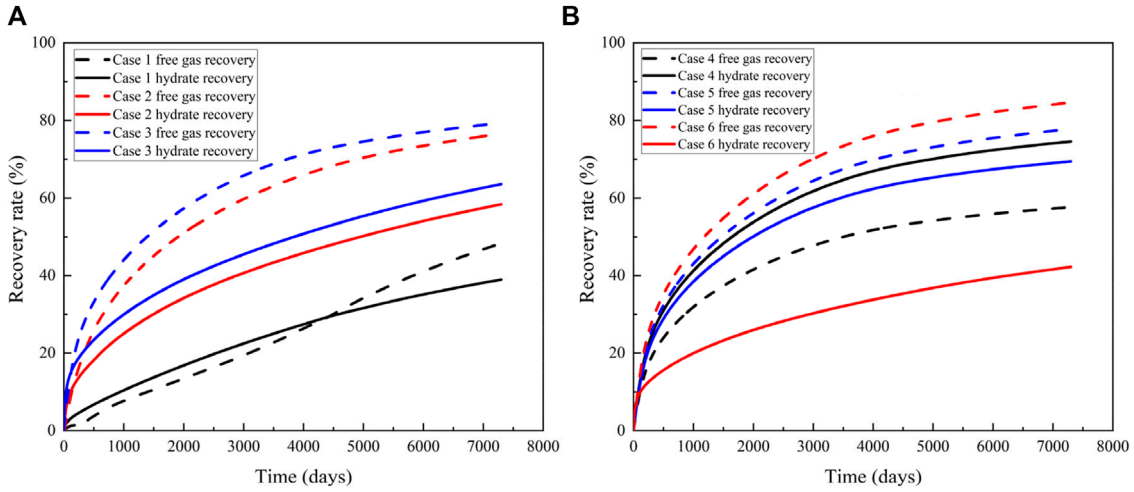

FIGURE 9
Recovery curves of free gas and hydrate from Cases 1–6. **(A)** Vertical well. **(B)** Horizontal well.

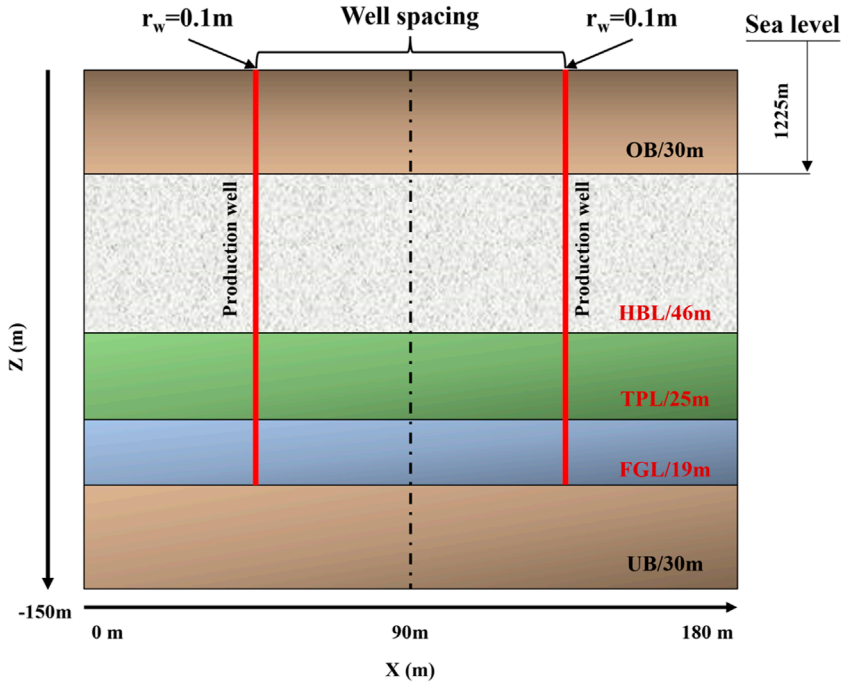

FIGURE 10
Schematic diagram of vertical wells with different well spacing for depressurization exploitation.

extraction effect is opposite to that of the hydrate two-phase layer, increasing the extraction range of the free gas layer but not directly contacting the upper hydrate layer. As a result, it only relies on the pressure drop transfer of the free gas layer to promote hydrate decomposition, which has a limited effect. The recovery rate of hydrate is 69.44%, and the recovery rate of free gas is 77.77%. The horizontal well arrangement can effectively connect the upper and lower layers, which can increase the decomposition area of hydrate and communicate with the lower free gas layer. Therefore, for long-term exploitation, it is recommended to drill horizontal wells to exploit the hydrate triple-phase layer, which can simultaneously exploit hydrate and free gas. Hence, the optimal option for straight well extraction is Case 3, and the optimal option for horizontal well extraction is Case 5.

4.3 Effect of well spacing

This section examines the impact of various vertical well spacing configurations on the recovery of hydrate and free gas. To illustrate, we select a symmetric cross section (x = 190 m) with a width of

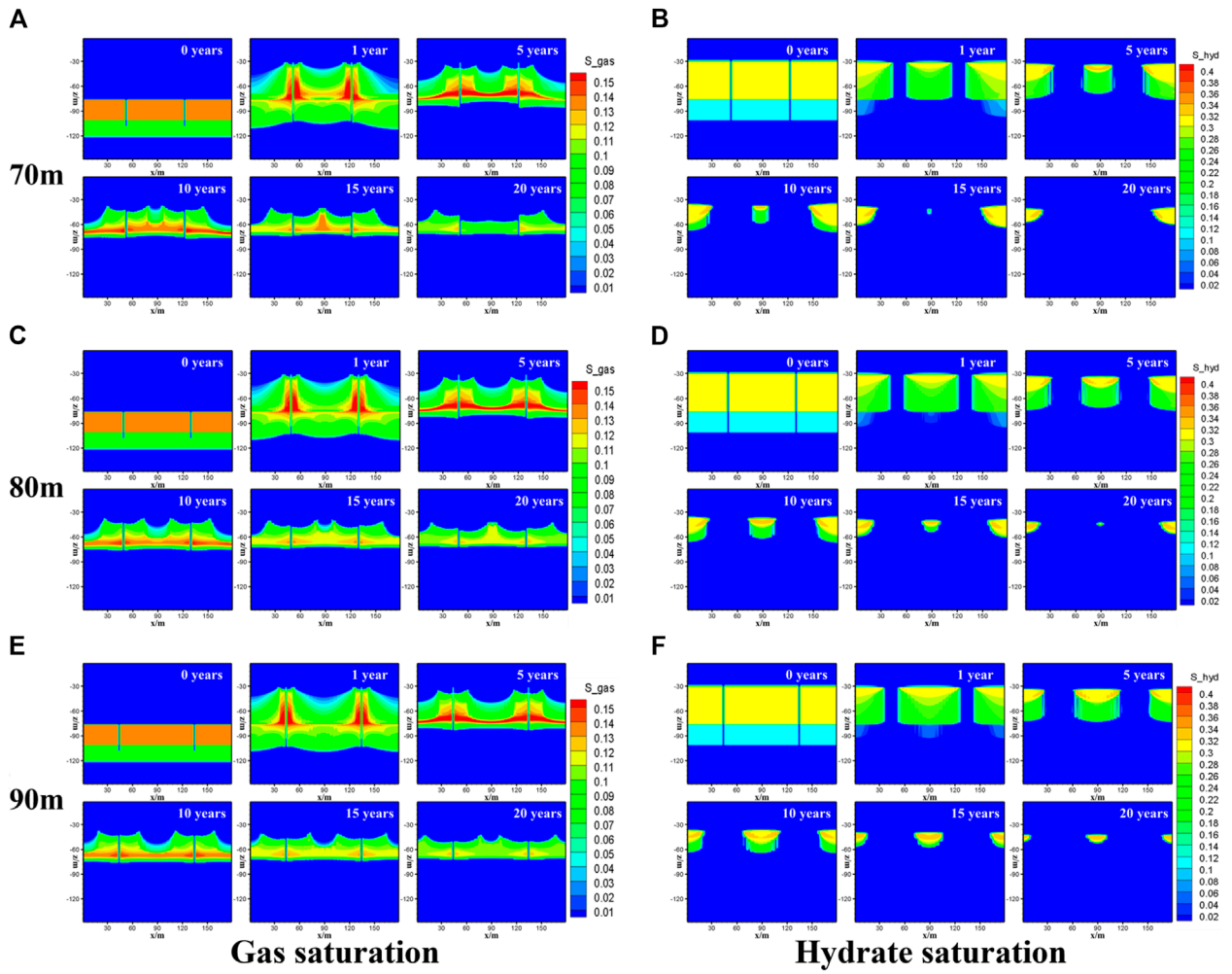

FIGURE 11
Spatiotemporal evolution of gas saturation field and hydrate saturation field, well spacing of 70–90 m. **(A, C, E)** Gas saturation Field. **(B, D, F)** Hydrate Saturation field.

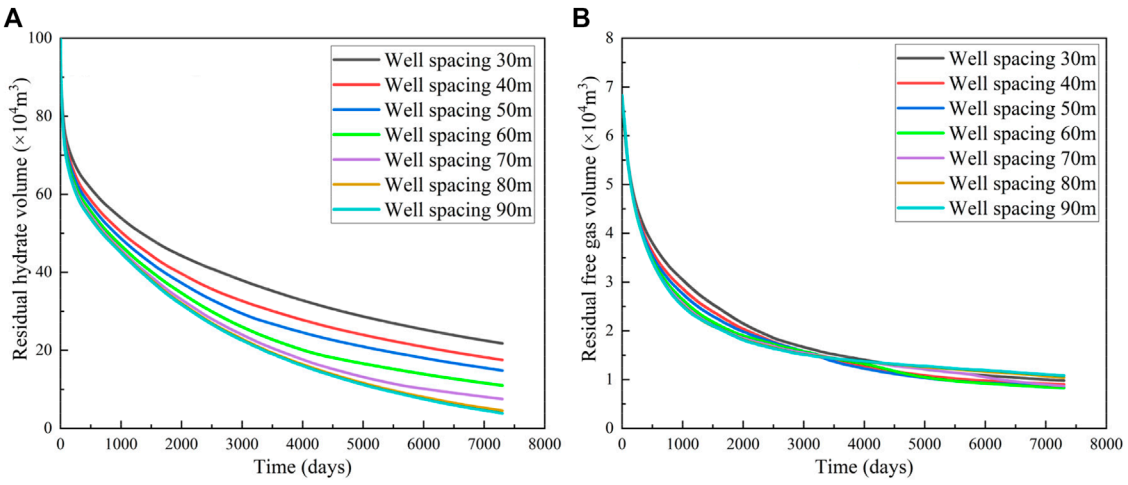

FIGURE 12
Variation trends of the residual hydrate volume and the residual free gas volume in depressurization exploitation with different well spacing for 20 years. **(A)** Residual hydrate volume. **(B)** Residual free volume.

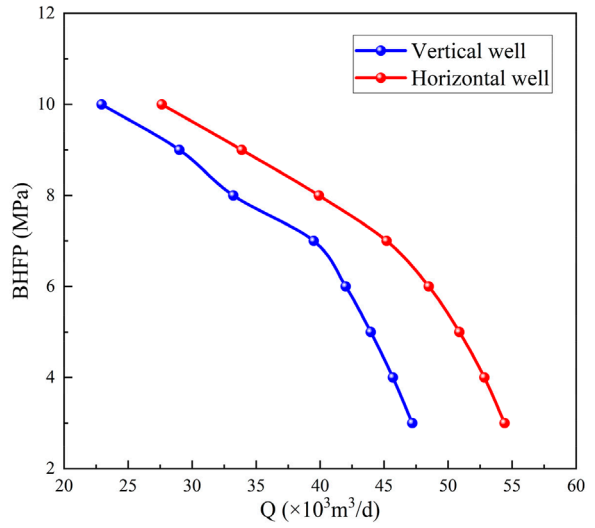

FIGURE 13
Inflow performance relationship curve.

1 m from the diameter of the model, as shown in Figure 10. The center of symmetry is positioned at x = 90 m, and we conduct depressurization exploitation simulations using vertical spacing of 30, 40, 50, 60, 70, 80, and 90 m to compare the variations of hydrate and free gas recovery rates under different vertical spacing configurations.

The spatial and temporal evolution of hydrate and free gas saturation extracted using depressurization at a well spacing of 30–60 m is shown in Supplementary Figures S1-S4. Figure 11 exhibit the spatial and temporal characteristics of hydrate and free gas saturation extracted using depressurization at a well spacing of 70–90 m. Figure 12 shows the variation trends of residual hydrate volume and residual free volume in 20 years of depressurized exploitation with different well spacing. As indicated in Figure 12A, the amount of residual hydrate extracted using double wells decreases gradually over time. The larger the spacing between double wells, the less residual hydrate is extracted after 20 years of operation. When the spacing between wells is 80 m and 90 m, the difference in the amount of residual hydrate is minimal. Combining the observations from Figure 11, it can be deduced that when the well spacing is 80 m, the undecomposed hydrate area between two wells is small, whereas when the well spacing is 90 m, the undecomposed hydrate area between two wells is larger. On the other hand, Figure 12B shows that the amount of residual free gas decreases rapidly initially, followed by a slower decline over time. However, the impact of different well spacing on the amount of residual free gas is not significant. To minimize the waste of hydrate resources, it is recommended to use double wells for hydrate exploitation in vertical wells with a well spacing of approximately 80 m.

4.4 Effect of bottom hole flowing pressure

The flow pressure at the bottom of the well is the most critical anthropogenic factor during pressure-reduction mining. Figure 13 displays the IPR (inflow performance relationship) curves for 20 years of vertical and horizontal well mining. Production capacity gradually declines as the bottom flow pressure rises, and at the same bottom flow pressure, the production capacity of horizontal wells is greater than that of vertical wells.

5 Conclusion

The specific purpose of this work is to conduct a numerical simulation study on depressurization exploitation for the class 1 hydrate reservoirs in the Shenhu sea of the South China Sea considering different development factors. In addition, the effects of different well types and different exploitation layers on the recovery rate of hydrate and free gas were analyzed. The effects of well spacing on enhanced hydrate recovery from vertical wells were also thoroughly investigated. Some important conclusions were drawn from the simulation results as below:

(1) For the first type of hydrate reservoir, under the same geological conditions, the highest hydrate and free gas recovery rates are achieved when mining to the free gas layer in a vertical well, which is the most effective approach. After 20 years of pressure-reduced extraction, the recovery rates of free gas and hydrate are 79.22% and 63.62%, respectively. The most effective approach is that the horizontal wells can extract hydrate and free gas at the same time when exploiting the hydrate three-phase layer. In the 2020 field test, the recovery efficiency of free gas from the optimal horizontal well is inferior to that from the optimal vertical well by 1.45%, but the recovery efficiency of hydrate is 5.82% higher than that from the vertical well. Since hydrate is more valuable to be extracted, the horizontal well is more effective.

(2) The best exploration efficiency is achieved when the spacing between two wells in a straight well is 80 m. In horizontal wells, the best recovery performance is achieved in the hydrate triple-phase layer. The recovery rates of free gas and hydrate were 77.77% and 69.44%, respectively, after 20 years of depressurization.

(3) The lower the flow pressure at the bottom of the well, the higher the production rate, but its influence is limited. Excessively low pressure will result in the hydrate layer freezing, so the bottomhole flow pressure should not be lower than the "four-phase point" of the hydrate phase equilibrium curve.

Data availability statement

The original contributions presented in the study are included in the article/Supplementary Material, further inquiries can be directed to the corresponding authors.

Author contributions

NW: Writing–review and editing, Funding acquisition, Resources. CL: Conceptualization, Data curation, Formal Analysis, Methodology, Software, Validation, Visualization, Writing–original draft, Writing–review and editing. XZ: Conceptualization, Data

curation, Formal Analysis, Methodology, Software, Validation, Visualization, Writing–original draft, Writing–review and editing. HL: Investigation, Writing–review and editing. LZ: Investigation, Writing–original draft, Writing–review and editing. JZ: Investigation, Writing–review and editing. BK: Funding acquisition, Project administration, Supervision, Writing–review and editing. RC: Funding acquisition, Methodology, Project administration, Supervision, Writing–review and editing.

Funding

The author(s) declare that financial support was received for the research, authorship, and/or publication of this article. This work was financially supported by the National Key Research and Development Program (Number 2021YFC2800903, 2023YFC2811002), National Natural Science Foundation of China (Number U20B6005-05), 111 Project (Number D21025), Open Fund Project of State Key Laboratory of Oil and Gas Reservoir Geology and Exploitation (Number PLN2021-01), and High-end Foreign Expert Introduction Program (Number G2021036005L).

Conflict of interest

The authors declare that the research was conducted in the absence of any commercial or financial relationships that could be construed as a potential conflict of interest.

Publisher's note

Supplementary material

The Supplementary Material for this article can be found online at: https://www.frontiersin.org/articles/10.3389/feart.2024.1444690/full#supplementary-material

References

Anderson, B. J., Kurihara, M., White, M. D., Moridis, G. J., Wilson, S. J., Pooladi-Darvish, M., et al. (2011). Regional long-term production modeling from a single well test, mount elbert gas hydrate stratigraphic test well, alaska north slope. *Mar. Pet. Geol.* 28, 493–501. doi:10.1016/j.marpetgeo.2010.01.015

Chen, L., Feng, Y. C., Okajima, J., Komiya, A., and Maruyama, S. (2018). Production behavior and numerical analysis for 2017 methane hydrate extraction test of Shenhu, south China sea. *J. Nat. Gas. Sci. Eng.* 53, 55–66. doi:10.1016/j.jngse.2018.02.029

Chibura, P. E., Zhang, W., Luo, A., and Wang, J. (2022). A review on gas hydrate production feasibility for permafrost and marine hydrates. *J. Nat. Gas. Sci. Eng.* 100, 104441. doi:10.1016/j.jngse.2022.104441

Cranganu, C. (2009). *In-situ* thermal stimulation of gas hydrates. *J. Pet. Sci. Eng.* 65, 76–80. doi:10.1016/j.petrol.2008.12.028

Fan, S. S., Yang, S. W., Wen, Y. G., Wang, Y. H., and Lang, X.-M. (2013). A simulation study of class III hydrate production with a high efficiency through the depressurization recovery and thermal stimulation in horizontal wells. *Nat. Gas. Ind.* 33, 36–42. (In Chinese). doi:10.3787/j.issn.1000-0976.2013.07.006

Feng, J. C., Wang, Y., Li, X. S., Li, G., Zhang, Y., and Chen, Z. Y. (2015). Production performance of gas hydrate accumulation at the GMGS2-site 16 of the pearl river mouth basin in the South China sea. *J. Nat. Gas. Sci. Eng.* 27, 306–320. doi:10.1016/j.jngse.2015.08.071

Gamwo, I. K., and Liu, Y. (2010). Mathematical modeling and numerical simulation of methane production in a hydrate reservoir. *Ind. Eng. Chem. Res.* 49, 5231–5245. doi:10.1021/ie901452v

Goel, N. (2006). *In situ* methane hydrate dissociation with carbon dioxide sequestration: current knowledge and issues. *J. Pet. Sci. Eng.* 51, 169–184. doi:10.1016/j.petrol.2006.01.005

Guo, X., Zhang, N., and Kong, B. (2022). Numerical simulation of depressurization production of natural gas hydrate in different well types. *Pet. Sci. Technol.* 41 (10), 1060–1080. doi:10.1080/10916466.2022.2072331

Hong, H. N., and Pooladi-Darvish, M. (2003) "A numerical study on gas production from formations containing gas hydrates," in *Proceeding of the Canadian international Petroleum Conference, PETSOC-2003-060, June 10–12, 2003, Calgary, Alberta, Canada; Canadian international petroleum conference*. Calgary, Alberta, Canada. doi:10.2118/2003-060

Konno, Y., Fujii, T., Sato, A., Akamine, K., Naiki, M., Masuda, Y., et al. (2017). Key findings of the world's first offshore methane hydrate production test off the Coast of Japan: toward future commercial production. *Energy fuels.* 31, 2607–2616. doi:10.1021/acs.energyfuels.6b03143

Kurihara, M., Sato, A., Ouchi, H., Narita, H., Masuda, Y., Saeki, T., et al. (2009). Prediction of gas productivity from Eastern Nankai Trough methane-hydrate reservoirs. *SPE Reserv. Eval. Eng.* 12, 477–499. doi:10.2118/125481-PA

Li, G., Li, X. S., Tang, L. G., and Zhang, Y. (2007). Experimental investigation of production behavior of methane hydrate under ethylene glycol injection in unconsolidated sediment. *Energy fuels.* 21, 3388–3393. doi:10.1021/ef060644d

Li, G., Li, X. S., Zhang, K., and Moridis, G. J. (2011). Numerical simulation of gas production from hydrate accumulations using a single horizontal well in Shenhu area, south China sea. *Chin. J. Geophys.* 54 (9), 2325–2337. (in Chinese). doi:10.3969/j.issn.0001-5733.2011.09.016

Li, J. F., Ye, J. L., Qin, X. W., Qiu, H. J., Wu, N. Y., Lu, H. L., et al. (2018). The first offshore natural gas hydrate production test in south China sea. *China Geol.* 1, 5–16. doi:10.31035/cg2018003

Lin, T. K., Dahyar, M., Lee, M. J., and Hsieh, B. Z. (2020). Study of the formation mechanisms of CO_2 hydrates from matching the experimental data with a porous media setting by multiphase flow-geochemical-thermal reservoir simulator. *J. Taiwan Inst. Chem. Eng.* 114, 115–124. doi:10.1016/j.jtice.2020.09.015

Makogon, Y. F., and Omelchenko, R. Y. (2013). Commercial gas production from messoyakha deposit in hydrate conditions. *J. Nat. Gas. Sci. Eng.* 11, 1–6. doi:10.1016/j.jngse.2012.08.002

Masuda, Y., Konno, Y., Iwama, H., Kawamura, T., Kurihara, M., and Ouchi, H. (2008) "Improvement of near wellbore permeability by methanol stimulation in a methane hydrate production well," in *Proceeding of the offshore Technology Conference, OTC-19433-MS, may 5–8, Houston, TX, USA; offshore Technology Conference*. Houston, TX, USA. doi:10.4043/19433-MS

McMullan, R. K., and Jeffrey, G. A. (1965). Polyhedral clathrate hydrates. IX. Structure of Ethylene Oxide hydrate. *J. Chem. Phys.* 42, 2725–2732. doi:10.1063/1.1703228

Merey, S., and Sinayuc, C. (2017). Numerical simulations for short-term depressurization production test of two gas hydrate sections in the black sea. *J. Nat. Gas. Sci. Eng.* 44, 77–95. doi:10.1016/j.jngse.2017.04.011

Moridis, G. J. (2003). Numerical studies of gas production from methane hydrates. *SPE J.* 8, 359–370. doi:10.2118/87330-PA

Moridis, G. J., and Collett, T. S. (2003) "Strategies for gas production from hydrate accumulations under various geologic conditions," in *Proceedings, TOUGH Symposium 2003*. Berkeley, CA, USA: Lawrence Berkeley national laboratory. May 12–14, 200.

Moridis, G. J., Kowalsky, M. B., and Pruess, K. (2007). Depressurization-induced gas production from class 1 hydrate deposits. *SPE Reserv. Eval. Eng.* 10, 458–481. doi:10.2118/97266-PA

Moridis, G. J., and Reagan, M. T. (2007a) "Gas production from oceanic class 2 hydrate accumulations," in *Proceeding of the offshore Technology Conference, OTC-18866-MS, April 30–may 3, Houston, TX, USA; offshore technology conference*. Houston, TX, USA. doi:10.4043/18866-MS

Moridis, G. J., and Reagan, M. T. (2007b) "Strategies for gas production from oceanic class 3 hydrate accumulations," in *Proceeding of the offshore Technology Conference, OTC-18865-MS, April 30–may 3, Houston, TX, USA; offshore technology conference: houston, TX, USA*. doi:10.4043/18865-MS

Moridis, G. J., and Reagan, M. T. (2011a). Estimating the upper Limit of gas production from class 2 hydrate accumulations in the permafrost: 1. Concepts, system Description, and the production Base case. *J. Pet. Sci. Eng.* 76, 194–204. doi:10.1016/j.petrol.2010.11.023

Moridis, G. J., and Reagan, M. T. (2011b). Estimating the upper limit of gas production from class 2 hydrate accumulations in the permafrost: 2. alternative well designs and sensitivity analysis. *J. Pet. Sci. Eng.* 76 (3-4), 124–137. doi:10.1016/j.petrol.2010.12.001

Moridis, G. J., Reagan, M. T., Boyle, K. L., and Zhang, K. (2011). Evaluation of the gas production potential of some particularly challenging types of oceanic hydrate deposits. *Porous Media* 90, 269–299. doi:10.1007/s11242-011-9762-5

Moridis, G. J., and Sloan, E. D. (2007). Gas production potential of disperse low-saturation hydrate accumulations in oceanic sediments. *Energy Conv. Manag.* 48, 1834–1849. doi:10.1016/j.enconman.2007.01.023

Myshakin, E. M., Gaddipati, M., Rose, K., and Anderson, B. J. (2012). Numerical simulations of depressurization-induced gas production from gas hydrate reservoirs at the walker ridge 313 site, northern Gulf of Mexico. *Mar. Pet. Geol.* 34, 169–185. doi:10.1016/j.marpetgeo.2011.09.001

Nair, V. C., Ramesh, S., Ramadass, G. A., and Sangwai, J. S. (2016). Influence of thermal stimulation on the methane hydrate dissociation in porous media under confined reservoir. *J. Pet. Sci. Eng.* 147, 547–559. doi:10.1016/j.petrol.2016.09.017

Ohgaki, K., Takano, K., Sangawa, H., Matsubara, T., and Nakano, S. (1996). Methane exploitation by carbon dioxide from gas hydrates—phase equilibria for CO_2-CH4 mixed hydrate system. *J. Chem. Eng. Jpn.* 29, 478–483. doi:10.1252/jcej.29.478

Qin, X. W., Liang, Q. Y., Ye, J. L., Yang, L., Qiu, H. J., Xie, W. W., et al. (2020). The response of temperature and pressure of hydrate reservoirs in the first gas hydrate production test in south China sea. *Appl. Energy.* 278, 115649. doi:10.1016/j.apenergy.2020.115649

Sloan, E. D., and Koh, C. A. (2007). *Clathrate hydrates of natural gases*. 3rd ed. New York: CRC Press. doi:10.1201/9781420008494

Su, Z., Moridis, G. J., Zhang, K., and Wu, N. Y. (2012). A huff-and-puff production of gas hydrate deposits in Shenhu area of south China sea through a vertical well. *J. Pet. Sci. Eng.* 86 (87), 54–61. doi:10.1016/j.petrol.2012.03.020

Sun, J. X., Qin, F. F., Ning, F. L., Gu, Y. H., Li, Y. L., Cao, X. X., et al. (2023). Gas recovery from silty hydrate reservoirs by using vertical and horizontal well patterns in the South China sea: effect of well spacing and its optimization. *Energy* 275, 127440. doi:10.1016/j.energy.2023.127440

Sun, Y. H., Ma, X. L., Guo, W., Jia, R., and Li, B. (2019). Numerical simulation of the short- and long-term production behavior of the first offshore gas hydrate production test in the south China sea. *J. Pet. Sci. Eng.* 181, 106196. doi:10.1016/j.petrol.2019.106196

Terzariol, M., and Santamarina, J. C. (2021). Multi-well strategy for gas production by depressurization from methane hydrate-bearing sediments. *Energy* 220, 119710. doi:10.1016/j.energy.2020.119710

Villano, L. D., Kommedal, R., Fijten, M. W. M., Schubert, U. S., Hoogenboom, R., and Kelland, M. A. (2009). A study of the kinetic hydrate inhibitor performance and seawater biodegradability of a series of Poly(2-alkyl-2-oxazoline)s. *Energy fuels.* 23, 3665–3673. doi:10.1021/ef900172f

Wang, D. Y., Ma, X. J., and Qiao, J. (2013). Impact factors of natural gas hydrate dissociation by depressurization: a review. *Adv. Mat. Res.* 868, 564–567. doi:10.4028/www.scientific.net/amr.868.564

Wei, N., Bai, R. L., Zhao, J. Z., Zhang, Y., and Xue, J. (2021). The prospect of natural gas hydrate (NGH) under the vision of peak carbon dioxide emissions in China. *Petroleum* 7, 357–363. doi:10.1016/j.petlm.2021.11.001

Wei, N., Pei, J., Zhao, J. Z., Zhang, L. H., Zhou, S. W., Luo, P. Y., et al. (2022). A state-of-the-art review and prospect of gas hydrate reservoir drilling techniques. *Front. Earth Sci.* 10. doi:10.3389/feart.2022.997337

Wei, N., Sun, W. T., Meng, Y. F., Liu, A. Q., Zhao, J. Z., Zhou, S. W., et al. (2018). Multiphase non equilibrium pipe flow behaviors in the solid fluidization exploitation of marine natural gas hydrate reservoir. *Energy Sci. Eng.* 6, 760–782. doi:10.1002/ese3.251

Xia, Z. Z., Wang, X. W., and Zhang, X. H. (2019). Investigation of the hydrate reservoir production under different depressurization modes. *Mar. Geores. Geotechnol.* 38 (8), 1002–1012. doi:10.1080/1064119X.2019.1646845

Xu, C. G., and Li, X. S. (2015). Research progress on methane production from natural gas hydrates. *RSC Adv.* 5, 54672–54699. doi:10.1039/c4ra10248g

Xu, C. G., Li, X. S., Yan, K. F., Ruan, X. K., Chen, Z. Y., and Xia, Z. M. (2019). Research progress in hydrate-based technologies and processes in China: a review. *Chin. J. Chem. Eng.* 27, 1998–2013. doi:10.1016/j.cjche.2018.12.002

Yamamoto, K. (2015). Overview and introduction: pressure core-sampling and analyses in the 2012-2013 MH21 offshore test of gas production from methane hydrates in the eastern nankai trough. *Mar. Pet. Geol.* 66, 296–309. doi:10.1016/j.marpetgeo.2015.02.024

Ye, J. L., Qin, X. W., Xie, W. W., Lu, H. L., Ma, B. J., Qiu, H. J., et al. (2020). The second natural gas hydrate production test in the South China sea. *China Geol.* 3, 197–209. doi:10.31035/cg2020043

Yu, T., Guan, G. Q., Abudula, A., Yoshida, A., Wang, D. Y., and Song, Y. (2019). Application of horizontal wells to the oceanic methane hydrate production in the nankai trough, Japan. *Jpn. J. Nat. Gas. Sci. Eng.* 62, 113–131. doi:10.1016/j.jngse.2018.11.027

Yu, T., Guan, G. Q., Wang, D. Y., Song, Y. C., and Abudula, A. (2021). Numerical evaluation on the effect of horizontal-well systems on the long-term gas hydrate production behavior at the second Shenhu test site. *J. Nat. Gas. Sci. Eng.* 95, 104200. doi:10.1016/j.jngse.2021.104200

Zhao, J., Song, Y., Lim, X. L., and Lam, W. H. (2017). Opportunities and challenges of gas hydrate policies with consideration of environmental impacts. *Renew. Sust. Energ. Rev.* 70, 875–885. doi:10.1016/j.rser.2016.11.269

Zhao, J. F., Yu, T., Song, Y. C., Liu, D., Liu, W. G., Liu, Y., et al. (2013). Numerical simulation of gas production from hydrate deposits using a single vertical well by depressurization in the Qilian Mountain permafrost, qinghai-tibet plateau, China. *Energy.* 52, 308–319. doi:10.1016/j.energy.2013.01.066

Zhao, J. F., Zhu, Z. H., Song, Y. C., Liu, W. G., Zhang, Y., and Wang, D. Y. (2015). Analyzing the process of gas production for natural gas hydrate using depressurization. *Appl. Energy.* 142, 125–134. doi:10.1016/j.apenergy.2014.12.071

Zhou, S. W., Chen, W., and Li, Q. P. (2014). The green solid fluidization development principle of natural gas hydrate stored in shallow layers of deep water. *China Offshore Oil Gas.* 26, 1–7. (In Chinese).

Zhou, S. W., Chen, W., Li, Q. P., Zhou, J. L., and Shi, H. S. (2017). Research on the solid fluidization well testing and production for shallow non-diagenetic natural gas hydrate in deep water area. *China Offshore Oil Gas.* 29, 1–8. (In Chinese). doi:10.11935/j.issn.1673-1506.2017.04.001

Zhou, S. W., Zhao, J. Z., Li, Q. P., Chen, W., Zhou, J. L., Wei, N., et al. (2018). Optimal design of the engineering parameters for the first global trial production of marine natural gas hydrates through solid fluidization. *Nat. Gas. Ind. B* 5, 118–131. doi:10.1016/j.ngib.2018.01.004